

Preparation and Electrochemical Performance of Porous Carbon from Fujimoto bean

Gaofeng Shi*, Zhao Wang, Chao Liu, Guoying Wang, Shiming Jia, Xia Jiang, Yucan Dong, Qi Zhang, Hongquan Zhang, Xin Li, Fenfang Luo

School of Petrochemical Engineering, Lanzhou University of Technology, Lan gong ping Road, Lanzhou, Gansu, China

*E-mail: 1042596082@qq.com

Received: 17 December 2018 / *Accepted:* 5 April 2019 / *Published:* 10 May 2019

In this paper, we report a method to prepare high-performance porous carbon from the high-yield Fujimoto bean by the process of chemical activation with KOH. The physicochemical properties of porous carbon were characterized by scanning electron microscopy, X-ray diffraction, nitrogen adsorption/desorption, Raman spectroscopy and X-ray photoelectron spectroscopy. The nitrogen adsorption/desorption test demonstrated that KOH has a good pore-making ability (maximum specific surface area of $1,159.95 \text{ m}^2 \cdot \text{g}^{-1}$ and a total pore volume of $0.60 \text{ cm}^3 \cdot \text{g}^{-1}$). The porous carbon exhibited excellent performance in symmetric double-layer capacitors, with a high specific capacitance of $219.8 \text{ F} \cdot \text{g}^{-1}$ at a current density of $2 \text{ A} \cdot \text{g}^{-1}$. When the current density increased from $1 \text{ A} \cdot \text{g}^{-1}$ to $10 \text{ A} \cdot \text{g}^{-1}$, the capacitance retention rate reached 84.73%; favourable cycle stability with 96.3% was maintained after 5,000 cycles at a current density of $2 \text{ A} \cdot \text{g}^{-1}$ in an aqueous electrolyte of 6 M KOH. At the same time, the material exhibited a higher energy density ($32.292 \text{ W} \cdot \text{h} \cdot \text{kg}^{-1}$) and power density ($500 \text{ W} \cdot \text{kg}^{-1}$). This result suggests that the porous carbon material could serve as an ideal electrode for supercapacitors.

Keywords: Fujimoto bean; supercapacitors; electrode; electrochemical performance

1. INTRODUCTION

Among many energy storage devices, a supercapacitor is a new type of energy storage medium that has attracted extensive attention because of its short charging time, reliable cycle stability, and good temperature characteristics, energy savings and environmental protection [1, 2]. The supercapacitor, also called an electrochemical capacitor, is based on the electrochemical double-layer theory [3, 4]. It can provide powerful pulse power. The energy is stored via the adsorption/desorption of electrolyte ions on the surface of electrode materials [5-9]. Until now, the main factor affecting

supercapacitor performance has been the electrode material [3, 10, 11]. Carbon-based materials are the most commonly employed electrode materials for supercapacitors and include activated carbon, graphene, carbon nanotubes, carbon nanofibres, carbon aerogels and carbide-derived carbons, all of which have been extensively developed for the supercapacitor [12-16]. Porous carbons, especially activated carbon with higher specific surface area, are the most widely adopted electrode materials for electric double-layer capacitors due to their good chemical stability, mature manufacturing technology, simple process and low price [17-19].

Carbon sources commonly used as porous carbon include biomass, domestic waste, and polymers. Gao [20] used rice husks as the carbon source for the preparation of porous carbon. The sample treated with KOH showed the highest specific capacitance of $174 \text{ F}\cdot\text{g}^{-1}$ in $\text{C}_8\text{H}_2\text{OBF}_4\text{N}$ electrolyte. Zhao [2] used abandoned mineral water bottles as a precursor. The sample treated with direct carbonization showed the highest specific capacitance of $176 \text{ F}\cdot\text{g}^{-1}$ at a current of $1 \text{ A}\cdot\text{g}^{-1}$ in 6 M KOH electrolyte. Chen [13] prepared a tobacco-derived activated carbon from tobacco waste using KOH activation. The result had a specific capacitance of $148 \text{ F}\cdot\text{g}^{-1}$ at a current density of $0.5 \text{ A}\cdot\text{g}^{-1}$.

In addition to the carbon sources mentioned above, starch has gradually become an area of research interest due to its high carbon content, easy obtainability, and complete biodegradation [21, 22]. The Fujimoto bean is a type of high-yield hybrid starch plant, it can grow for many years once sown and can blossom and bear pods every day. It can also be transplanted with flowers or beans. No chemical fertilizers and pesticides are needed in the planting process, which is beneficial to environmental protection. Despite of the high yield of the Fujimoto bean, it has a low utilization rate because they are not directly edible by people or livestock. The issue of how to make full use of this high-yield leguminous plant and increase its additional value has great prospects for research and development.

Therefore, it is necessary to explore a new way to meet new requirements of biomass-sources and environment protection. In this paper, carbon materials were prepared through carbonization and KOH activation of Fujimoto bean. Further, the microstructure of the prepared porous carbon materials was characterized. The results indicate that the microstructure of the prepared carbon materials is highly dependent on the activation ratio. The activation ratio also has a strong influence on the electrochemical properties of the carbon materials. As an electrode material, the sample showed the highest specific capacitance of $205 \text{ F}\cdot\text{g}^{-1}$ at a current of $2 \text{ A}\cdot\text{g}^{-1}$ and cyclic stability (96.3% capacitance was retained after 5,000 charge-discharge cycles under $2 \text{ A}\cdot\text{g}^{-1}$ current density) in 6 M KOH electrolyte.

2. EXPERIMENTAL

2.1. Experimental method

Fujimoto beans were crushed to a powder of particle size less than 100 mesh. KOH was analytically pure. Porous carbon was prepared by KOH activation by mixing the Fujimoto bean powder with KOH. The as-prepared white powdered sample was mixed with KOH in different mass ratios (its mass ratio was 1:0, 2:1, 1:1, 1:2 compared with the Fujimoto bean powder and KOH) and

crushed in an agate mortar for 30 minutes, followed by heating at 900°C for 1.5 h; the heating ratio was 5°C per minute in a N₂ gas atmosphere. Then, the black solid was thoroughly washed with 2 M HCl solution. Eventually, the carbon was dried at 80°C for 12 h in an oven. The porous carbon is denoted herein according to the expression PC-X, where PC-1 is the mass ratio of Fujimoto bean powder to KOH of 1:0, PC-2 is the mass ratio of Fujimoto bean powder to KOH of 2:1, PC-3 is the mass ratio of Fujimoto bean powder to KOH of 1:1 and PC-4 is the mass ratio of Fujimoto bean powder to KOH of 1:2. The process for the preparation of the porous carbon is shown in Figure 1.

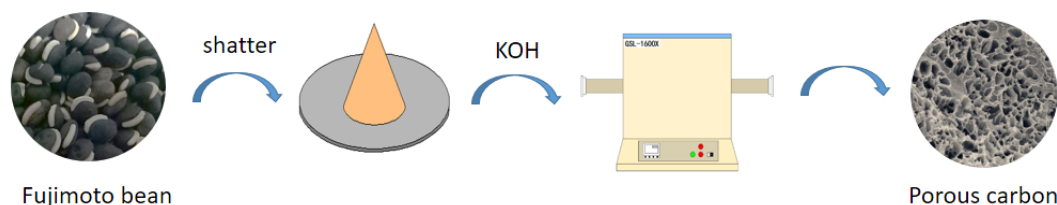


Figure 1. Preparation process of porous carbon.

2.2. Structure characterization

The surface structure of the porous carbon was observed by cold field emission type scanning electron microscope (SEM, JSM-6701F Japan Electron Optics Co., Ltd.). The pore size distribution and specific surface area of the samples were tested by adsorption and desorption of nitrogen gas in a Micromeritics ASAP 2420 surface analyzer by using the Brunauer-Emmett-Teller (BET). The MSA-XD2 powder X-ray diffractometer was used to test the crystal structure of the material (diffraction angle scanning range is 5 to 80°). Raman spectrum was evaluated by spectrometer (JYHR800, Micro-Raman). Surface composition was tested with an X-ray photoelectron spectroscopy (XPS, PHI5702, USA).

2.3 Test of electrochemical properties.

The electrochemical performance measurements were carried out on a CHI660E electrochemical work station (CHI660E, Shanghai Chenhua Instrument Co., Ltd.) in 6 M KOH aqueous electrolyte with a conventional three-electrode configuration. The obtained sample, acetylene black, and polytetrafluoroethylene (PTFE) were uniformly mixed at a mass ratio of 80%, 15%, and 5%, respectively, to prepare a working electrode. The slurry was then loaded onto a piece of nickel foam (1.0×2.0 cm) and dried at 80°C for 12 h in a vacuum oven. Then, the electrode sheet was formed under a pressure of 5 MPa. Cyclic voltammetry (CV), galvanostatic charge–discharge (CP), and impedance (EIS) were performed on an electrochemical workstation using a saturated calomel electrode (SCE) and a platinum foil as a reference electrode and a counter electrode, respectively. The CV tests were conducted with a potential range of -1.0 V to 0 V by varying the scan rate from 5 m·Vs⁻¹ to 100 m·Vs⁻¹. The CP tests were conducted with a potential range of -1 V to 0 V at a current density

from $1 \text{ A}\cdot\text{g}^{-1}$ to $10 \text{ A}\cdot\text{g}^{-1}$. Electrochemical impedance spectroscopy (EIS) tests were performed in a frequency range from 0.01 Hz to 100000 Hz at open circuit potential. The specific capacitance C ($\text{F}\cdot\text{g}^{-1}$), energy density E ($\text{W}\cdot\text{h}\cdot\text{kg}^{-1}$) and power density P ($\text{W}\cdot\text{kg}^{-1}$) were calculated using the following formulae:

$$C = \frac{I\Delta t}{m\Delta V} \quad (1)$$

$$E = \frac{1}{2} C\Delta V^2 \quad (2)$$

$$P = \frac{E}{t} \quad (3)$$

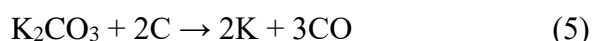
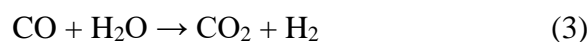
Where I denotes the discharge current, Δt (t) is the discharge time, m is the mass load, ΔV (V) is the potential window of discharge, E is the energy density and P is power density [13, 23] .

3. RESULT AND DISCUSSION

3.1 SEM analysis of porous carbon.

The morphology and size were observed by SEM. After KOH activation, the porous carbon exhibited an irregular shape, and a massive structure and a rough outer surface appeared. Figure 2 shows a scanning electron microscope image of the prepared PC-1 and PC-3 samples at a magnification of 5,000. It can be seen from the figure that with the addition of KOH, the degree of graphitization is reduced and the degree of amorphousness is increased. It can also be seen from the figure that the degree of graphitization is reduced with the addition of KOH. This surface structure facilitates ion storage and migration of the KOH electrolyte, rapidly forming an electric double-layer on the surface thereof. As a result, PC-3 samples may exhibit extremely high specific capacity and excellent electrochemical performance.

During the activation heating process, a series of reactions occur [24]:



K_2CO_3 forms at approximately 400°C , and KOH is completely consumed at approximately 600°C under the condition of sufficient carbon. In the activation process, various potassium compounds, such as K_2O and K_2CO_3 , act as activators and react with carbon to form pore structures. The gases H_2 , H_2O , CO or CO_2 produced in the reaction also contribute to the formation of pores. When the temperature exceeds 760°C , metallic potassium may be produced according to reactions 5 and 6 [19, 25] . K gasification added to steam diffusion into the interior of the Fujimoto bean powder can cause distortion of the carbon layer. Subsequently, during the 900°C heat preservation process, the activation process would continue until the $\text{K}/\text{K}_2\text{CO}_3/\text{CO}_2$ reaction with carbon comes to a halt.

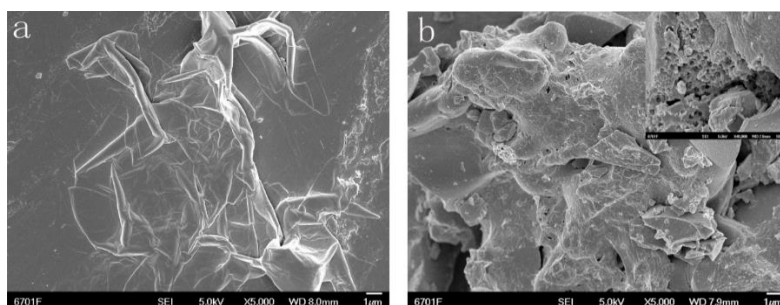


Figure 2. SEM micrographs of (a) PC-1 and (b) PC-3.

3.2 XRD and Raman analysis of porous carbon.

To further examine the structures of all the samples, XRD characterization was performed. Figure 3 (a) shows a crystal structure diagram of different amounts of KOH added. Two broad characteristic peaks appeared at 22.5° and 44° for the four samples, corresponding to the (002) crystal plane and the amorphous carbon (100) crystal plane, respectively, of the graphite layer [26, 27]. The broad characteristic peaks appeared at 22.5° for the four samples, corresponding to the (002) crystal plane indicating a disturbed structure due to the randomly oriented aromatic carbon sheets in the obtained carbons, which is major factor for high specific surface area [28]. The other broad peak, located at approximately 44° , may be attributed to the amorphous carbon (100) crystal plane of the graphite layer, which is suggested for improving the electrical conductivity of carbon [29].

Raman spectroscopy was further employed to analyse the microstructure of the prepared carbon specimen. Figure 3 (b) shows Raman test results for the four samples. It can be seen from the figure that there are two distinct characteristic peaks D and G in the spectrum, where D peak represents the disordered structure of carbon material and G peak represents the graphitized structure. The intensity ratio of D band to G band (ID/IG) can reflect the degree of structural disorder in the carbon materials, and the degree of graphitization of the carbon matrix was analysed [30, 31]. The IG/ID values corresponding to samples PC-1, PC-2, PC-3, and PC-4 were 1.184, 1.175, 1.167, and 1.162, respectively. As shown Fig. 3, with the increase in KOH mass, the degree of graphitization decreased, which is basically consistent with the previous XRD analysis results. It is affected by its crystallinity structure, which is good for the fast transmission of electrolyte ions, thus promoting ion diffusion and improving the capacitive performance of the porous carbon material.

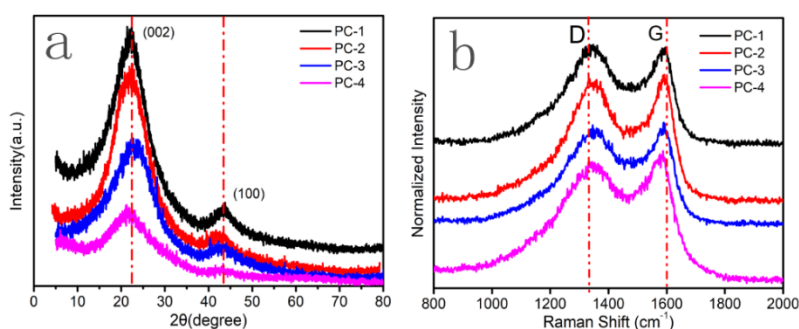


Figure 3. (a) XRD patterns of four samples, (b) Raman spectra of four samples.

3.3 Specific surface area and pore structure of porous carbon.

To study the effect on the microstructure of the material, we performed nitrogen adsorption-desorption characterization on all samples, and the results are shown in Figure 4 (a). The N₂ adsorption-desorption isotherm of the porous carbon showed a typical hybrid of type IV according to the International Union of Pure and Applied Chemistry (IUPAC) classification, indicating the coexistence of micropores and mesopores. At low relative pressure ($P/P_0 < 0.1$), there was strong nitrogen adsorption, and the adsorption curve rose slowly at medium and high pressures, indicating the existence of the microporous structure. When $P/P_0=0.4$, a significant hysteresis loop appeared, indicating that there were a large number of mesopores [32, 33]. Figure 4 (b) shows the pore size distribution (PSD) curves for the porous carbon by using the Barrett Joyner-Halenda (BJH) method. All the porous carbon samples exhibited abundant micropore structures.

The microstructures of KOH/porous carbon in different proportions are shown in Table 1. It can be seen from the table that the specific surface area of the sample PC-3 was $1,159.95 \text{ m}^2 \cdot \text{g}^{-1}$, and the specific surface area of the micropores was $904.81 \text{ m}^2 \cdot \text{g}^{-1}$, which accounts for 78% of the total specific surface area. The total pore volume was $0.60 \text{ cm}^3 \cdot \text{g}^{-1}$, and the micropore volume was $0.42 \text{ cm}^3 \cdot \text{g}^{-1}$, which accounted for 69.2% of the total pore volume. The results indicate that the structure of porous carbon is mainly a microporous structure.

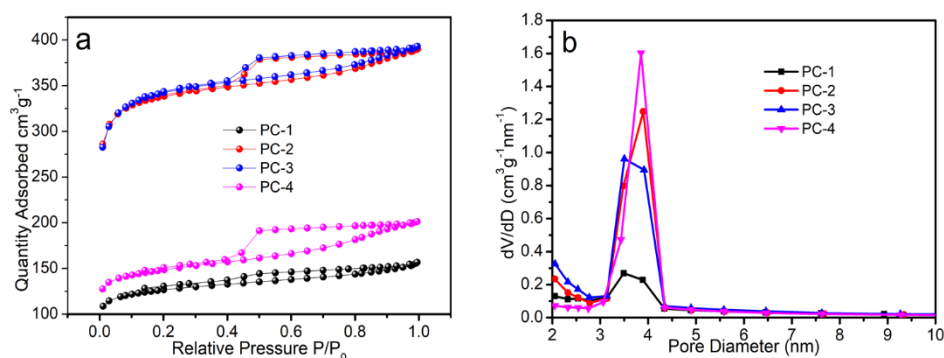


Figure 4. (a) N₂ adsorption/desorption isotherms and (b) the BJH pore size distribution curves of the porous carbons.

Table 1. Pore size distribution of porous carbon

| Sample | $S_{\text{BET}}^{\text{a}}$ $\text{cm}^2 \cdot \text{g}^{-1}$ | V_{c}^{b} $\text{cm}^3 \cdot \text{g}^{-1}$ | $D_{\text{ave}}^{\text{c}}$ nm | $V_{\text{mic}}^{\text{d}}$ $\text{cm}^3 \cdot \text{g}^{-1}$ | $V_{\text{ext}}^{\text{e}}$ $\text{cm}^3 \cdot \text{g}^{-1}$ | $S_{\text{mic}}^{\text{f}}$ $\text{cm}^2 \cdot \text{g}^{-1}$ | $S_{\text{ext}}^{\text{h}}$ $\text{cm}^2 \cdot \text{g}^{-1}$ |
|--------|--|--|-----------------------------------|--|--|--|--|
| PC-1 | 427.48 | 0.249 | 2.22 | 0.15 | 0.09 | 322.09 | 105.40 |
| PC-2 | 1142.38 | 0.59 | 2.09 | 0.43 | 0.17 | 929.38 | 212.99 |
| PC-3 | 1159.95 | 0.60 | 2.08 | 0.42 | 0.18 | 904.81 | 255.14 |
| PC-4 | 501.72 | 0.31 | 2.45 | 0.17 | 0.13 | 374.75 | 126.98 |

a: surface area b: total pore volume c: average pore diameter d: Micropore volume e: External volume f: Micropore surface area g: External surface area

3.4 XPS elemental analysis of porous carbon.

To determine the elemental composition and bonding of the sample, we performed X-ray photoelectron spectroscopy (XPS) analysis on sample PC-3. The C, O, N, and P element in the PC-3 sample were analyzed, where in the C content was 92.66 wt%, the O content was 7.07 wt%, the N content was 0.19 wt%, and the P content was 0.008 wt%. It indicates that the content of the N and P elements of the porous carbon is scarce.

For the C1s XPS spectrum, the PC-3 sample can be fitted with three curves. Three different peaks located at ~ 284.6 eV, ~ 285.5 eV and ~ 289.3 eV correspond to the sp² hybrid (C=C, C-C), C-O bonding and carboxyl or ester groups (O-C=O), respectively [1]. For the O1s XPS spectrum, the PC-3 sample can be fitted with three curves. Three different peaks located at ~ 531.6 eV, ~ 532.7 eV and ~ 533.7 eV correspond to C=O bonding, single-bond oxygen (-O-) in the C-O group and carboxyl or ester groups (O-C=O), respectively. In general, the bonding form is mainly combined with O=C-O [13]. The C elements are all present in the form of oxygen-containing functional groups. The presence of oxygen-containing functional groups on the surface of the material not only improves the surface hydrophilicity of the electrode material but also improves the electrochemical properties of the material itself.

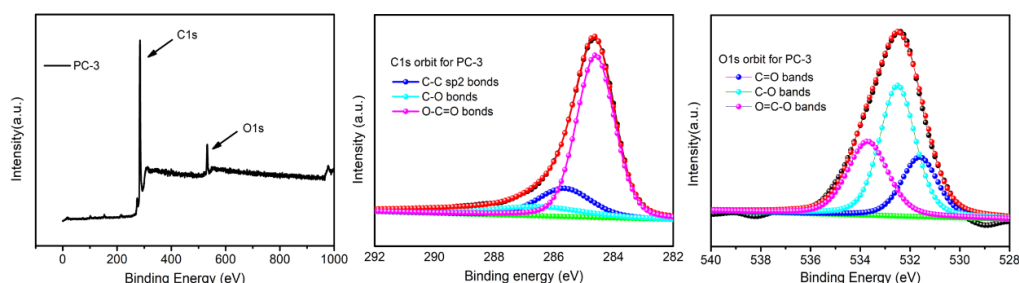


Figure 5. XPS full peak, C1s and O1s spectra of the PC-3 sample.

3.5 Electrochemical properties

The typical CV curves of all samples at a scan rate of $20 \text{ mV}\cdot\text{s}^{-1}$ in the potential window from -1.0 V to 0 V are shown in Figure 6 (a). All samples show a quasi-rectangular shape in their CV curves, suggesting an expected electrical double-layer capacitance behaviour based on the adsorption and exchange of electrolyte ions. It can be observed that the CV curve area of the PC-1 sample is significantly smaller than that of other doped KOH, indicating that the KOH-activated sample has a large charge storage capacity, in turn indicating the best energy storage performance. It is seen that as the mass ratio of Fujimoto bean powder to KOH increases, the closed area of the CV curve first increases and then decreases, indicating that the PC-3 sample has the largest curve area. Figure 6 (b) shows the specific capacitance of the different samples at a current density of $2 \text{ A}\cdot\text{g}^{-1}$. Under normal circumstances, the charging and discharging curves of the constant current charging and discharging curve of the ideal electric double-layer capacitor are symmetrically distributed and have a triangular shape without a significant voltage drop. For all samples, the linear curves with symmetrical charge

and discharge lines indicate the good capacitive behaviour. At $2 \text{ A}\cdot\text{g}^{-1}$ current density, the specific capacitances tested for PC-1, PC-2, PC-3, and PC-4 were $154.4 \text{ F}\cdot\text{g}^{-1}$, $198.3 \text{ F}\cdot\text{g}^{-1}$, $219.8 \text{ F}\cdot\text{g}^{-1}$ and $218.2 \text{ F}\cdot\text{g}^{-1}$, respectively. It is shown that the discharge time of the CP curve first increases and then decreases with an increase of KOH, which is consistent with the results of the CV curve. Figure 6 (c) shows the CV curve of PC-3 at different scan rates from $5 \text{ mV}\cdot\text{s}^{-1}$ to $100 \text{ mV}\cdot\text{s}^{-1}$ in the potential window from -1.0 V to 0 V . Even at a high scan rate of $100 \text{ mV}\cdot\text{s}^{-1}$, the CV curve can still maintain a rectangular shape, suggesting its good reversibility, fast charge/discharge ability and good ion transport ability.

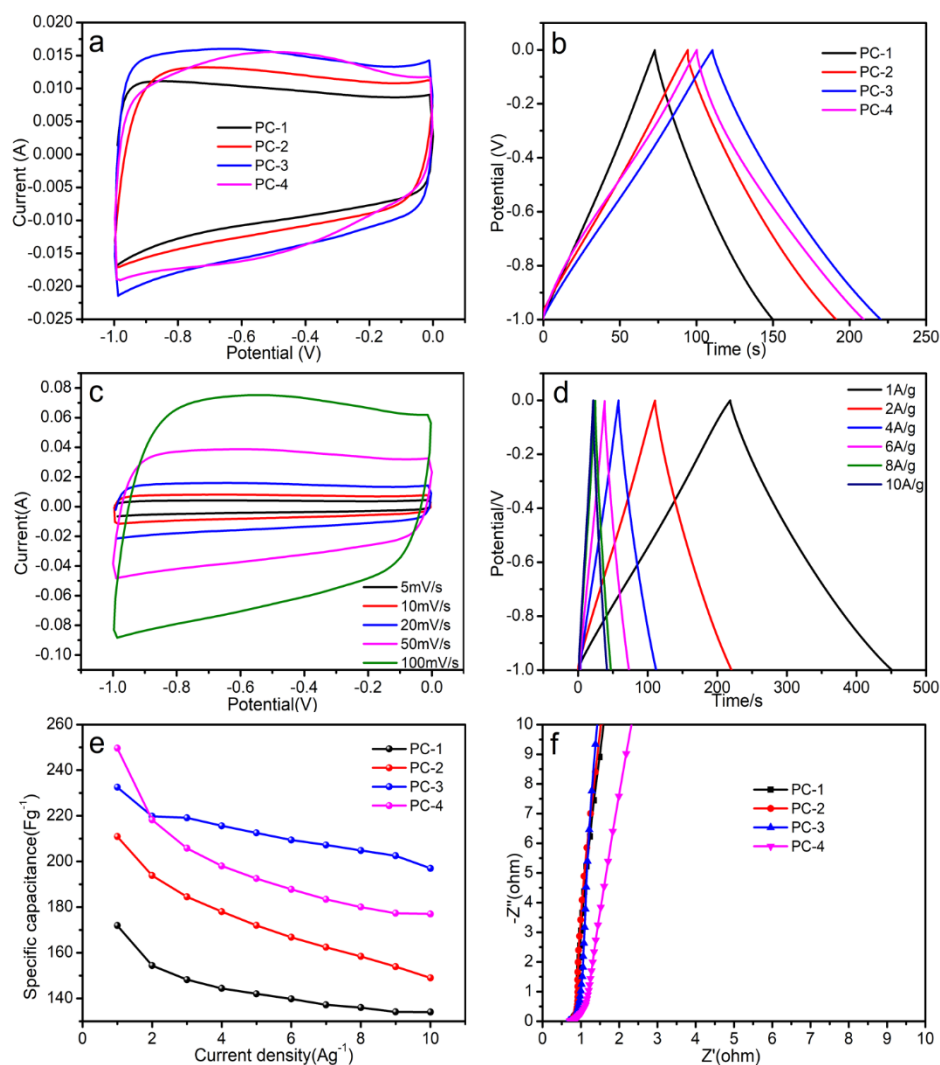


Figure 6. Electrochemical performance of the samples measured in a three-electrode system. (a) CV curves for all the samples at a scan rate of $20 \text{ mV}\cdot\text{s}^{-1}$; (b) galvanostatic charge-discharge curves of all the samples at the current density of $2 \text{ A}\cdot\text{g}^{-1}$; (c) CV curves for PC-3 at scan rates ranging from $5 \text{ mV}\cdot\text{s}^{-1}$ to $100 \text{ mV}\cdot\text{s}^{-1}$; (d) galvanostatic charge-discharge curves of PC-3 at different current densities; (e) specific capacitance of the samples versus various current densities from $1 \text{ A}\cdot\text{g}^{-1}$ to $10 \text{ A}\cdot\text{g}^{-1}$; (f) Electrochemical impedance spectra(EIS) of the PC-3;

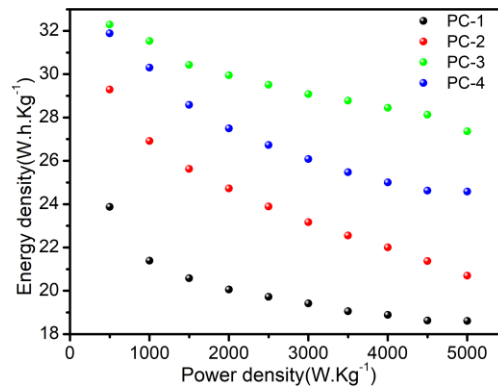


Figure 7. Energy and power density of four samples.

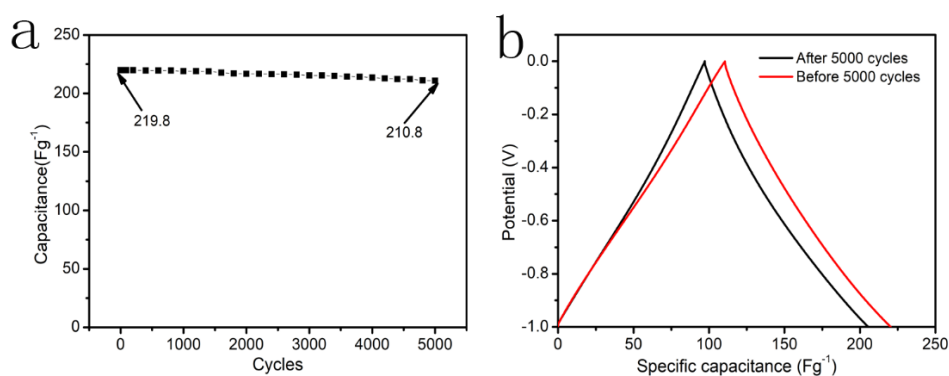


Figure 8. PC-3 in specific capacitance retention rates at the current density of 2 A·g⁻¹ after 5000 cycle.

Table 2. Specific capacitance of porous carbon (F·g⁻¹)

| Current density (A·g ⁻¹) | 1 | 2 | 4 | 6 | 8 | 10 |
|--------------------------------------|-------|-------|-------|-------|-------|-----|
| PC-1 | 171.9 | 154.4 | 144.4 | 139.8 | 136 | 116 |
| PC-2 | 210.9 | 193.8 | 178 | 166.8 | 158.4 | 149 |
| PC-3 | 232.5 | 219.8 | 215.6 | 209.4 | 202.5 | 197 |
| PC-4 | 229.6 | 218.2 | 198 | 187.8 | 180 | 177 |

Table 3. Comparison of electrochemical performance of porous carbon with other different materials

| Electrode materials | Specific capacitance (current density) | Electrolyte | Referencces |
|--|--|---------------------------|-------------|
| porous carbon based on cationic starch | 238 F·g ⁻¹ (0.37 A·g ⁻¹) | 30wt% KOH | [34] |
| porous carbon based on potato starch | 245 F·g ⁻¹ (1 A·g ⁻¹) | 1 mol·L ⁻¹ KOH | [23] |
| porous carbon based on corn starch | 162 F·g ⁻¹ (0.652 A·g ⁻¹) | 6 mol·L ⁻¹ KOH | [35] |
| porous carbon based on Fujimoto bean | 232.5 F·g ⁻¹ (1 A·g ⁻¹) | 6 mol·L ⁻¹ KOH | This work |

Figure 6 (d) shows the specific capacitance of PC-3 at different current densities. It can be concluded from the figure that the prepared porous carbon charge and discharge curve is a symmetrical triangle, indicating good capacitive behaviour. As the current density increases, the area of the curve exhibits a decreasing trend because the transport of electrolyte ions in the pores is limited at high current densities. In Figure 6 (e) and Table 2, when the current density increases from $1 \text{ A}\cdot\text{g}^{-1}$ to $10 \text{ A}\cdot\text{g}^{-1}$, the specific capacitances of PC-1, PC-2, PC-3, and PC-4 samples are reduced. The initial values are 67.95%, 70.65%, 84.73%, and 77.09%, respectively. PC-3 shows the best rate of magnification in all samples. Thus, it can be seen that KOH activation promotes the rate performance of the sample. As shown in Fig. 6 (f), we can see an approximately vertical straight line of the samples, indicating that the electrolyte solution has good transport and diffusion properties inside the prepared material. The nearly vertical lines in the low-frequency range reveal a typical capacitive behaviour of the samples, while the slight deviation from the ideal vertical line can be assigned to the result of the pore size distribution [3, 27]. Figure 7 shows that at the same current density, porous carbon PC-3 exhibits the highest current density and power density. The energy density is $32.292 \text{ W}\cdot\text{h}\cdot\text{kg}^{-1}$ at a power density of $500 \text{ W}\cdot\text{kg}^{-1}$, and the energy density is $27.362 \text{ W}\cdot\text{h}\cdot\text{kg}^{-1}$ at a power density of $5,000 \text{ W}\cdot\text{kg}^{-1}$. That indicates that it has good electrical conductivity, promotes electron transfer, and contributes to an increase in energy density. Fig. 8 shows the PC-3 sample cycle characteristics at a current density of $2 \text{ A}\cdot\text{g}^{-1}$. It can be seen from the figure that after 5,000 cycles of charge and discharge, the specific capacitance of PC-3 is $208.8 \text{ F}\cdot\text{g}^{-1}$ and the retention rate is 96.3%, indicating that the sample has an excellent electrochemical cycle stability. The above analysis shows that due to the excellent capacitance performance of PC-3, it may be used as a supercapacitor electrode material.

To evaluate the superiority of the prepared electrode materials, Table 3 lists our results compared to previously published preparations of porous carbon by starch.

4. CONCLUSIONS

Porous carbon materials were prepared through carbonization and KOH activation of the Fujimoto bean. The morphology, microstructure and electrochemical properties of porous carbon under different activation conditions were investigated. Meanwhile, by controlling the amount of KOH added, the sample PC-3 with the best electrochemical performance was obtained. When the current density was $1 \text{ A}\cdot\text{g}^{-1}$, the specific capacitance of porous carbon was $232.5 \text{ F}\cdot\text{g}^{-1}$, the energy density was $32.292 \text{ W}\cdot\text{h}\cdot\text{kg}^{-1}$, the power density was $500 \text{ W}\cdot\text{kg}^{-1}$, and the capacitance retention rate was 84.73%, which demonstrates a good rate performance. After charging and discharging for 5,000 cycles, the capacitance value was maintained at 96.3%, which indicates the obtained has an excellent cycle stability. The PC-3 sample has a high specific surface area and has a large number of micropores. The novel preparation method has many advantages, including low toxicological effects of materials and processes, ecologically friendly biomaterials and simple technology. The successful development of this method not only improves the added value of biomass energy but also makes full use of renewable energy sources.

ACKNOWLEDGEMENTS

This work was supported by the National Natural Science Foundation of China (21567015), the National Key Research and Development Program of China (2016YFC0202900), Lanzhou university of technology hongliu first-class discipline construction program (Support) and Lanzhou university of technology Hongliu Science Fund for Young Scholars (2018 Support).

References

1. C. Lu, Y.H. Huang, Y.J. Wu, J. Li and J.P. Cheng, *J. Power Sources*, 394 (2018) 9.
2. X. Zhao, P. Li, S.W. Yang, Q.Z. Zhang and H.M. Luo, *Ionics*, 23 (2017) 1239.
3. H. Jin, J.P. Hu, S.C. Wu, X.L. Wang, H. Zhang, H. Xu and K. Lian, *J. Power Sources*, 384 (2018) 270.
4. N.T. Li, S.C. Tang, Y.N. Dai and X.K. Meng, *J. Mater. Sci.*, 49 (2014) 2802.
5. Z.S. Zhang, Y.F. Zhang, K. Yang, K.Y. Yi, Z.H. Zhou, A.P. Huang, K.C. Mai and X.H. Lu, *J. Mater. Chem. A*, 3 (2015) 1884.
6. B.G. Choi, J. Hong, W.H. Hong, P.T. Hammond and H. Park, *ACS Nano*, 5 (2011) 7205.
7. X.J. He, P.H. Ling, M.X. Yu, X.T. Wang, X.Y. Wang and M.D. Zheng, *Electrochim. Acta*, 105 (2013) 635.
8. L.L. Shi, L.H. Jin, Z. Meng, Y.N. Sun, C. Li and Y.H. Shen, *ACS. Adv.*, 8 (2018) 39937.
9. Y.H. Cao, K.L. Wang, X.M. Wang, Z.R. Gu, Q.H. Fan, W. Gibbons, J.D. Hoefelmeyer, P.K. Khared and M.Shrestha, *Electrochim. Acta*, 212 (2016) 839.
10. A. Alabadi, X.J. Yang, Z.H. Dong, Z. Li and B. Tan, *J. Mater. Chem. A*, 2 (2014) 11697.
11. Z.A. Xiao, W.W. Chen, K. Liu, P. Cui, D. Zhan, *Int J. Electrochem Sci.*, 13 (2018) 5370.
12. X.J. He, Z.D. Liu, H. Ma, N. Zhang, M.X. Yu and M.B. Wu, *Microporous Mesoporous Mater.*, 236 (2016) 134.
13. H. Chen, Y.C. Guo, F. Wang, Q. Wang, P.R. Qi, X.H. Guo, B. Dai and F. Yu, *New Carbon Materials.*, 32 (2017) 592.
14. D.H. Tang, S. Hu, F. Dai, R. Yi, M.L. Gordin, S.R. Chen, J.X. Song and D.H. Wang, *ACS Appl. Mater. Interfaces*, 8 (2016) 6779.
15. S. Han, D.Q. Wu, S. Li, F. Zhang and X.L. Feng, *Adv. Mater.*, 26 (2014) 849.
16. L. Hao, X.L. Li and L.J. Zhi, *Adv. Mater.*, 25 (2013) 3899.
17. M. Sevilla and R. Mokaya, *Energy Environ. Sci.*, 7 (2014) 1250.
18. L. Wei and G. Yushin, *Nano Energy*, 1 (2012) 552.
19. Y.W. Zhu, S. Murali, M.D. Stoller, K.J. Ganesh, W.W. Cai, P.J. Ferreira, A. Pirkle, R.M. Wallace, K. A. Cychosz, M. Thommes, D. Su, E.A. Stach and R.S. Ruoff, *Science*, 332 (2011) 1537.
20. Y. Gao, L. Li, Y.M. Jin, Y. Wang, C.J. Yuan, Y.J. Wei, G. Chen, J.J. Ge and H.Y. Lu, *Appl. Energy*, 153 (2015) 41.
21. S. Zhao, C.Y. Wang, M.M. Chen and Z.Q. Shi, *Mater. Lett.*, 62 (2008) 3322.
22. S. Zhao, C.Y. Wang, M.M. Chen, Z.Q. Shi and N Liu, *New Carbon Materials.*, 25 (2010) 438.
23. R.B. Qiang, Z.A. Hu, Y.Y. Yang, Z.M. Li, A. Ning, X.Y. Ren, H.X. Hu and H.Y. Wu, *Electrochim. Acta*, 167 (2015) 303.
24. G.B. Lou, Y.T. Wu, X.Q. Zhu, Y.Z. Lu, S. Yu, C.H. Yang, H. Chen, C. Guan, L. Li and Z.H. Shen, *ACS Appl. Mater. Interfaces*, 49 (2018) 42503.
25. R.T. Wang, P.Y. Wang, X.B. Yan, J.W. Lang, C. Peng and Q.J. Xue, *ACS Appl. Mater. Interfaces*, 4 (2012) 5800.
26. C. Ma, R.R. Wang, Z.Y. Xie, H.X. Zhang, Z.Y. Li and J.L. Shi, *J. Porous Mater.*, 24 (2017) 1437.
27. S.J. Lei, L.F. Chen, W. Zhou, P.Q. Deng, Y. Liu, L.F. Fei, W. Lu, Y.H. Xiao and B.C. Cheng, *J. Power Sources*, 379 (2018) 74.
28. L. Zhang, F. Zhang, X. Yang, K. Leng, Y. Huang and Y.S. Chen, *Small*, 9 (2013) 1342.

29. J.P. Paraknowitsch, J. Zhang, D.S. Su, A. Thomas and M. Antonietti, *Adv. Mater.*, 22 (2010) 87.
30. X.D. Hao, J. Wang, B. Ding, Y. Wang, Z. Chang, H. Dou and X.G. Zhang, *J. Power Sources*, 352 (2017) 34.
31. J.N. Yi, Y. Qing, C.T. Wu, Y.X. Zeng, Y.Q. Wu, X.H. Lu and Y.X. Tong, *J. Power Sources*, 351 (2017) 130.
32. H.L. Lu, W.J. Dai, M.B. Zheng, N.W. Li, G.B. Ji and J.M. Cao, *J. Power Sources*, 209 (2012) 243.
33. Y.J. Ou, C. Peng, J.W. Lang, D.D. Zhu and X.B. Yan, *New Carbon Materials*, 77 (2014) 1196.
34. H.Q. Wang, Y.L. Qing, Q.Y. Li, J.H. Yang and Q.F. Dai, *J. Phys. Chem. Solids*, 69 (2008) 2420.
35. L.Y. Pang, B. Zou, X. Han, L.Y. Cao, W. Wang, Y.P. Guo, *Mater. Lett.*, 184 (2016) 88.

© 2019 The Authors. Published by ESG (www.electrochemsci.org). This article is an open access article distributed under the terms and conditions of the Creative Commons Attribution license (<http://creativecommons.org/licenses/by/4.0/>).